CONTAIN CALCULATIONS OF DEBRIS CONDITIONS ADJACENT TO THE BWR MARK I DRYWELL SHELL DURING THE LATER PHASES OF A SEVERE ACCIDENT

CONF-8810155--19

DE89 003179

C. R. Hyman

Boiling Water Reactor Severe Accident
Technology (BWRSAT) Program*
Oak Ridge National Laboratory

For presentation at
16th Water Reactor Safety Information Meeting
October 27, 1988

DISCLAIMER

*Research sponsored by the Office of Nuclear Regulatory Research, U.S. Nuclear Regulatory Commission under Interagency Agreement DOE 0551-0551-A1 with the U.S. Department of Energy under contract DE-AC05-840R21400 with the Martin Marietta Energy Systems, Inc.

CONTAIN CALCULATIONS OF DEBRIS CONDITIONS ADJACENT TO THE BWR MARK I DRYWELL SHELL DURING THE LATER PHASES OF A SEVERE ACCIDENT

C. R. Hyman

Oak Ridge National Laboratory
Oak Ridge, Tennessee 37831

ABSTRACT

Best estimate CONTAIN calculations have recently been performed by the BWR Severe Accident Technology (BWRSAT) Program at Oak Ridge National Laboratory to predict the primary containment response during the later phases of an unmitigated low-pressure Short Term Station Blackout at the Peach Bottom Atomic Power Station. Debris pour conditions leaving the failed reactor vessel are taken from the results of best estimate BWRSAR analyses that are based upon an assumed metallic debris melting temperature of 2750°F (1783 K) and an oxide debris melting temperature of 4350°F (2672 K). Results of the CONTAIN analysis for the case without sprays indicate failure of the drywell head seals due to the extremely hot atmospheric conditions extant in the drywell. The maximum calculated temperature of the debris adjacent to the drywell shell is less than the melting temperature of the shell, yet the sustained temperatures may be sufficient to induce primary containment pressure boundary failure by the mechanism of creep-rupture. It is also predicted that a significant portion of the reactor pedestal wall is ablated during the period of the calculation. Nevertheless, the calculated results are recognized to be influenced by large modeling uncertainties. Several deficiencies in the application of the CORCON module within the CONTAIN code to BWR severe accident sequences are identified and discussed.

1. INTRODUCTION

This paper provides a discussion of recent containment analyses performed by the ORNL BWRSAT Program to estimate the primary containment response during the later phases of an unmitigated Short-Term Station Blackout at Peach Bottom. The work was performed at the request of Dr. Thomas J. Walker, Leader of the Task Group on the BWR Mark I Shell Melt-Through Issue established by the Accident Evaluation Branch of the Nuclear Regulatory Commission (NRC) Office of Nuclear Regulatory Research. The tool used to perform this containment analysis is a modified version of the most recent release of the CONTAIN code.[1]

The invessel and debris release portions of this accident sequence were analyzed by the BWRSAR code and provide the subject of a separate paper presented at this meeting.[2] The debris pours and the primary containment initial conditions used in the CONTAIN analysis were taken from the BWRSAR results. Principal characteristics of the BWRSAR calculated debris pours are: (1) the debris leaves the reactor vessel in a discontinuous manner over a period of 11 h, (2) early debris pours are mainly metallic (Fe, Cr, Ni, Zr) with a characteristic melting temperature of 2750°F (1783 K), and (3) later debris pours are primarily oxide (ZrO_2, UO_2) with a melting temperature of 4350°F (2672 K). Figure 1 shows the calculated total mass flow and temperature of the debris as it leaves the reactor vessel. This information was taken from Reference 2.

The following Section describes the modeling approach used to perform the containment analysis with CONTAIN, Section 3 presents results, Section 4 provides a discussion of current deficiencies in the CONTAIN/CORCON linkage with respect to BWR accident analyses, while Section 5 presents a summary.

2. BWR MARK I PRIMARY CONTAINMENT MODELING APPROACH

2.1 ORNL CONTAIN Model

The BWRSAT Program at ORNL has developed a 12-cell CONTAIN model for use in analysis of the response of the BWR Mark I primary containment under severe accident conditions. The model is shown in Fig. 2. Cells one through nine are used to represent the free volume of the drywell. Core debris/concrete interactions are calculated with the CORCON module of CONTAIN for the floor of Cell 1 after the initial debris pour from the reactor vessel and also for the floor of Cell 6 when the debris has spread into the expedestal region. Cell 7 represents the one-foot (0.305 m) wide annular region between the outer surface of the reactor insulation and the inner surface of the concrete biological shield. Flow paths through the reactor pedestal and biological shield are indicated by dotted lines; as shown, they connect Cells 1 and 6, 2 and 5, 3 and 4, 7 and 4, and 7 and 9.

Cell 10 of the model is a large single-cell representation of the secondary containment, both reactor building and refueling bay. Its purpose is to trap leakage flows from the drywell shell either by temporary lifting of the drywell head or by temperature-induced failure of the drywell shell at the level of the floor. Cell 11 represents the outside environment and collects any gases that escape from the secondary containment (cell 10) or are vented from the primary containment via the wetwell airspace, which constitutes Cell 12 of the model.

2.2 Debris Spreading Methodology

The currently released version of the CONTAIN code allows for the time dependent addition of debris mass onto the drywell floor and the calculation of the subsequent debris/concrete interaction via the CORCON module. The

debris/concrete reaction is calculated for a well-defined user input "crucible" geometry, but no allowance is made for consideration of a time dependent lateral spreading of molten core debris across a flat floor, such as would be expected to occur in the BWR Mark I drywell. Accordingly, the code user must attempt to simulate debris spreading by stopping and restarting the calculation. It is the purpose of this Section to explain the rationale behind performing multiple CONTAIN calculations, with each calculation considering increasing areas of the drywell floor being affected by the debris/ concrete interaction.

Because the initial debris pour from the reactor vessel as defined by the BWRSAR calculation is metallic, lasts for only 30 minutes, and has very little superheat [Temp = 2750°F (1783 K)], the debris freezes on the drywell floor and is not able to spread. In addition, the initial debris pour barely fills the drywell sump [Volume = 206 ft^3 (5.83 m^3)] and thus physically would not be able to spread throughout the drywell. The time between termination of the first pour and the beginning of the second pour is approximately 1 h. It is reasonable therefore to consider an initial debris/concrete interaction that is confined to the inpedestal region of the drywell. Thus, for the purpose of analyzing the initial debris/concrete reaction, a "crucible" geometry representative of the inpedestal region of the drywell floor was assumed.

According to the BWRSAR calculation, the initial pour begins at time 263 min. after scram and is terminated at time 298 minutes. Starting at about 360 min., a second debris pour is predicted; this pour is a mixture of oxides and metals that exits the vessel at a temperature higher than that of the first pour. The second debris pour is added to the floor debris already present, and the mixed debris temperature begins to rise rapidly.

By time 375 min., the height of the debris in the inpedestal region extends 3.1 in. (0.08 m) above the drywell floor level. In addition, the oxide portion of the debris has been sufficiently diluted by concrete slag oxides (SiO_2,CaO) so that the oxide solidus temperature is lowered to 2523°F (1657 K). The oxide temperature at this time is 2655°F (1730 K). Thus, a reason exists for increasing the debris/concrete interaction area being analyzed by CORCON in order to simulate the increased interaction area caused by probable debris spreading into the expedestal area of the drywell floor. The question that remains to be answered is: How large a radius is appropriate for initial debris spreading into the expedestal area? Also, once the extent of initial expedestal debris spreading has been determined, a separate CONTAIN calculation must be initiated as CONTAIN cannot be instructed by user input to perform the simple maneuver of moving debris from the debris/concrete interaction occurring in one cell to another cell and to begin a new debris/ concrete interaction calculation in the new cell.

Using the method proposed by Kazimi[3] to estimate the extent of initial debris spreading over the expedestal floor, it was determined for these calculations that the initial spread area in the expedestal region should be 800 $ft.^2$ (74.3 m^2). Therefore, a second CONTAIN calculation was initiated with debris/concrete interactions continuing on the inpedestal floor [322 ft^2 (27.9 m^2) - Cell 1] and beginning on the expedestal floor [800 ft^2 (74.3 m^2) -

Cell 6]. The results of this calculation showed that after only three additional minutes the debris conditions on the expedestal floor were appropriate for further spreading over the remaining 300 ft^2 (27.9 m^2) of the expedestal region.

The short duration of the second calculation is caused by the very rapid pour from the failed reactor vessel during this period (Fig. 1), the large superheat of the molten metals assumed to flow into the expedestal area, and the large expedestal energy release from chemical reaction of zirconium with gases released by the ablation of concrete. Thus, the expedestal debris is predicted to accumulate rapidly and to remain molten.

During the three minute period of the initial debris spread into the expedestal region, the metals portion of the continuing pour from the reactor vessel is predicted by BWRSAR to be molten and superheated, while the oxide portion of the pour is frozen. Accordingly, it was assumed that 80% of the oxide pour remained inpedestal while 20% of the oxide pour was injected directly into the expedestal region. For the metals, it was assumed that one percent was kept inpedestal due to adhesion upon the surfaces of the frozen oxides. An exception was made for the zirconium metal to model its eutectic formation with the oxides; an additional 10% of the zirconium metal was kept inpedestal so that only 89% of this metal was directed into the expedestal region.

After time 378 min., when the debris expedestal is modeled to spread over the entire 1100 ft^2 (102.2 m^2) of expedestal floor area, the apportionment of the continuing debris pour from the reactor vessel between the inpedestal and expedestal areas remained the same as before; the basis being that the metals continued to be molten and superheated while the oxides were frozen.

After time 515 min., the oxide debris pour is molten as well as the metals. Thus, there is no reason to preferentially retain oxides in the inpedestal region. From this time until the end of the calculation at 900 min., the apportionment of the predicted debris pour was made strictly according to the respective floor areas; thus, 23% was kept inpedestal and 77% was introduced into the expedestal region.

As a summary of the above, three CONTAIN calculations were required to perform the analyses discussed in this paper. The first CONTAIN calculation is used to estimate events during the period from 255 to 375 min. and corresponds to the debris/concrete interaction period when the debris resides on the inpedestal region of the drywell floor. The second CONTAIN calculation, only three minutes long (375 to 378 min.), corresponds to the initial spreading of debris onto the expedestal floor. Simultaneous debris/concrete interactions are analyzed both inpedestal and expedestal with CORCON being independently active in both Cells 1 and 6 (see Fig. 2). As modeled by user input to the BWRSAR calculation that allocates the pours between the inpedestal and expedestal regions, inpedestal debris sources are rich in frozen oxides while expedestal sources are rich in molten metals.

The final calculational period from 378 until 900 min. constitutes the domain of the third CONTAIN calculation. Again, simultaneous but independent inpedestal and expedestal debris/concrete interactions were calculated, but this time the debris/concrete interaction area for the expedestal calculations was increased from 800 ft^2 (74.3 m^2) to the full expedestal floor area of 1100 ft^2 (102.2 m^2). For times prior to 515 min., the reactor vessel debris pours predicted by BWRSAR are comprised of frozen oxides and molten metals. Therefore, the inpedestal debris sources again are rich in frozen oxides while the expedestal sources are rich in molten metals. After 515 min., both the metal and oxide flows from the vessel are molten, and debris sources of uniform composition are added to the inpedestal and expedestal floor areas.

2.3 Assumptions Regarding Lifting of the Drywell Head

The model for lifting of the drywell head is taken from the discussion beginning on page 58 of the recently completed Chicago Bridge and Iron Company study of Peach Bottom containment strength (Ref. 4). In recent gasket tests at Idaho National Engineering Laboratory (Ref. 5), gaskets similar to those used at Peach Bottom withstood differential pressures of 160 psi (1.103 MPa) combined with temperatures of 700°F (644 K), but then failed catastrophically as the temperature was increased to 730°F (661 K). Greg Krueger of PECo has confirmed that the drywell head gaskets at Peach Bottom are replaced each refueling. Then, with the assumption of normal (0.04 in.) gasket springback, a leakage area would not ordinarily begin to open until the drywell pressure reached 175 psia (1.207 MPa).[4] However, recognizing that the results of the CONTAIN calculations discussed here involve drywell head temperatures well in excess of 700°F (644 K), a leakage area is assumed to open for these calculations when the temperature of the drywell head reaches 730°F (661 K). As modeled, the leakage area increases linearly from zero at 97 psia (0.669 MPa) to a value of 62 $in.^2$ (0.04 m^2) as the pressure increases to 215 psia (1.482 MPa).

3. CALCULATED RESULTS

Table 1 presents the limestone common sand concrete composition used at Peach Bottom and the composition of high limestone concrete. As seen from this table, limestone common sand concrete contains less carbon dioxide than high limestone concrete. In addition, it has an ablation temperature [2246°F (1503 K)] significantly lower than that of high limestone concrete [2694°F (1752 K)]. The reader should keep these considerations in mind as the results presented in this section would be significantly altered by a change in concrete types.

The CONTAIN calculation was initiated just before reactor vessel bottom head penetration failure (255 min.) with the initial drywell cell temperatures taken from BWRSAR code results, and the CORCON calculation of the debris/concrete interaction was initiated 10 minutes later. The intercell flows and cell temperatures 10 min. after bottom head penetration failure and the beginning of gas release from the depressurized reactor vessel into the drywell are

shown in Figs. 3a and 3b, respectively. The highest atmosphere temperature, as expected, is in the uppermost inpedestal cell, immediately beneath the reactor vessel. As shown in Fig. 3a, two natural circulation flows are set up by the calculation: a clockwise flow between the inpedestal and lower expedestal region, and a counter-clockwise flow between the upper expedestal region and annular Cell 7 that represents the volume between the reactor vessel and the biological shield.

Primary containment atmospheric temperatures and flows at time 593 min., which is immediately after leakage from the drywell head flange seals is expected to begin, are shown in Fig. 4. The high temperatures that occur at this time are due to continuous concrete ablation, the associated gas release into the debris, the metal oxidation therein, and the escape into the atmosphere of gases sparged through the debris. The gas temperature in Cell 8 is high enough at this time that the temperature of the heat sink representing the drywell head is predicted to exceed 730°F (661 K).

As explained in Section 2.3, the drywell head seals are modeled to fail catastrophically once they reach 730°F (661 K). Because the drywell pressure, Fig. 5, is 126 psia (0.869 MPa), the head is modeled to be lifted at this time so that a leakage area of 15.5 $in.^2$ (0.010 m^2) ensues when the seals fail. This leakage directly enters the refueling bay and therefore bypasses the reactor building. It is represented in Fig. 4a as an arrow leaving Cell 8. Once the head seals fail, the drywell pressure decreases to about 98 psia (0.68 MPa). This pressure is representative of the maximum pressure that could be maintained if the drywell head had no seals. A small leakage flow continues to occur until the end of the calculation at 900 min. as the debris/concrete interaction continues to release gas into the drywell atmosphere and thus provides a continuous pressure source to maintain a small flange separation.

The configuration of the debris layers on the drywell floor just before and just after initial spreading into the expedestal region are shown in Table 3. In particular, it can be noted that ablation of the inpedestal concrete is significant. The bottom of the debris sinks from −7.71 inches (floor of the original sump configuration) to −16.26 inches during the period 265–375 min.

Radial concrete ablation in the inpedestal region as calculated by CONTAIN is significant, as shown in Fig. 6, which indicates the maximum radius of the lowest inpedestal cell as a function of time. The plotted curve begins when the CORCON calculation is initiated, at time 265 min. The initial value of 10.125 ft (3.09 m) is the radius to the inner pedestal in its original configuration. Pedestal ablation is most rapid during the early part of the calculation, when zirconium oxidation is occurring. About seven percent of the original pedestal width is predicted to be consumed during the period prior to the initial spread into the expedestal region.

Comparison of the radial concrete ablation shown in Fig. 6 to the axial ablation shown in Table 3 reveals that the predicted radial ablation at the time (375 min.) of initial spread into the expedestal region is much less than the predicted axial ablation (0.2 ft radial vs 0.7 ft axial).

There are two reasons for this. First, the lower portion of the inpedestal debris consists of a relatively thin layer of frozen metals so that the resistance to heat transfer by conduction in the radial direction is much larger than the resistance in the axial direction. Second, although there is no appreciable radial crust in the partially liquified layer of oxides overlying the metals, the convective heat transfer in the radial direction is limited in this layer by the stable gas film maintained at the interface between the debris and the concrete. Because the gas flow in this vertical film at the outer radius of the debris is laminar, the CORCON module assigns a Nusselt number (1.0) close to the Nusselt number (0.804) used for the horizontal gas film at the base of the frozen metallic layer. Since both of these Nusselt numbers are defined directly in terms of the gas film thickness, the thicker gas film at the vertical interface results in a convective heat transfer coefficient smaller than that for the horizontal interface, where the gas film is much thinner. Thus, the predicted downward heat transfer and ablation exceeds the radial heat transfer and ablation.

The debris/concrete interaction begins in the expedestal region at 375 min., just after the debris inpedestal has accumulated to a sufficient depth and molten state to be modeled to flow through the pedestal doorway. As explained in Section 2.2, the initial expedestal area covered by this debris flow is 800 ft^2 (74.3 m^2). Since the entire expedestal floor area is only 1100 ft^2 (102.2 m^2), this initial spreading area supports the contention that the entire expedestal floor area would be covered quickly, especially in light of the large debris pour rate leaving the reactor vessel at this time and the large amount of superheat associated with the metals flowing to the expedestal region of the floor. Indeed, only three additional minutes of pour produce conditions for which the spreading debris would completely cover the expedestal floor.

The expedestal debris temperatures are shown in Fig. 7. They reach their maximum values during the period from 375 to 430 min. These high temperatures are calculated because of the oxidation of zirconium metal as it is being added to the expedestal floor area. A comparison of energy release rates due to chemical and decay heat sources is provided in Fig. 8. Chemical power is much larger than decay power during the period before exhaustion of the zirconium metal at time 435 min. and clearly is the reason for the calculated high debris temperatures expedestal during this period.

As discussed in Section 2, the debris source to the expedestal region of the drywell floor is metals-rich during the period between the initial spread into this region and the time when the temperature of the vessel pour is sufficient to result in molten oxides. During this 140-min. period from time 375 to time 515 min., 89% of the zirconium and 99% of the other metals in the ongoing pour are directed into the expedestal region. For the oxides in the pour, which are frozen during this period, 80% are modeled by CONTAIN code input to flow into the inpedestal region while 20%, assumed to be carried into the expedestal region with the molten metal flow, are directed into the expedestal region.

It is obviously important to consider to what extent the calculated debris temperatures in the expedestal region are dependent upon the assumed division of metals and oxides between the inpedestal and expedestal regions of the drywell floor. To this end, the pour partitioning was redone so that both metals and oxides were split between the inpedestal and expedestal regions strictly on the basis of the respective floor areas and the CONTAIN calculation of the drywell response was repeated. This exercise was performed both for the three-minute period immediately following the initial spread into the expedestal region, when the pour is divided between the 322 ft^2 (29.9 m^2) of the inpedestal region and 800 ft^2 (74.3 m^2) of the expedestal region, and for the final spread over the entire expedestal region.

The expedestal debris temperatures for this uniform debris composition case are shown on Fig. 9a and 9b, together with the temperatures for the best-estimate case. The overall temperature profiles for the two predictions have similar shapes. For the metal layer (Fig. 9a), the peak temperature is slightly higher for the uniformly distributed case, but the period during which the temperature remains elevated is correspondingly shorter. This is consistent with the assumed partitioning of the debris pours.

From time 378 to 515 min., the best-estimate expedestal debris pour is rich in metals, incorporating 89% of the molten zirconium and 99% of the molten stainless steel leaving the reactor vessel, but only 20% of the frozen oxides. During the same period, 77% of the metals and 77% of the oxides in the ongoing pour are directed into the expedestal region for the uniform composition case. Thus, the best-estimate calculation places more zirconium metal in the expedestal region and the predicted chemical energy source and the debris temperatures remain elevated longer than in the uniform case calculation.

On the other hand, the additional oxides added to the expedestal region in the uniform composition case overlie the metals and reduce the heat loss from the metal layer to the atmosphere. This causes the peak metal layer temperature to be slightly higher for the uniform composition case and, over the long term, the predicted temperature of the metal layer for this case remains about 50°F (28 K) higher than the metal layer temperature for the best-estimate metals-rich case.

In neither calculation does the predicted expedestal debris temperature exceed the melting temperature of the carbon steel drywell shell [2800°F (1810 K)] and, as indicated on Figs. 9a and 9b, the calculated temperature profiles are similar. Thus, although assumptions regarding the degree of lateral separation of the molten metals from the frozen oxides have some effect upon the calculated expedestal debris temperatures, these assumptions clearly are not the dominant parameters in determining the question of shell survivability.

The cumulative gas release from the concrete is provided in Table 2 for the limestone common sand concrete considered in this paper. It should be noted that most of the carbon dioxide and steam released from the concrete is consumed in metal-gas reactions within the debris; relatively little of these

gases escapes from the debris surface to enter the drywell atmosphere. It should also be noted that of the 1717 lb-moles released from the debris, 66% is hydrogen and 28% is CO. Thus, 94% of the released debris gas is combustible. This has important ramifications regarding the performance of the secondary containment if the primary containment fails.

A final threat to primary containment integrity is posed by the significant predicted erosion of the reactor pedestal illustrated by Fig. 6. As discussed earlier, about seven percent of the reactor pedestal is predicted to be eroded at the time of initial spreading of debris into the expedestal region. An additional 23% of the original pedestal is predicted to be eroded by the end of the calculation. However, this predicted 30% reduction in pedestal wall thickness is probably a minimum estimate since the attack upon the pedestal wall from the other side by the expedestal debris (after time 375 min.) is not considered in the calculation.

Table 4 provides the time-history of the conditions at the debris-shell interface as calculated by CONTAIN for the periods during which the metal and oxide temperatures in the expedestal region are sufficiently high to challenge the integrity of the shell. As shown on Fig. 7, these temperatures approach the melting temperature of carbon steel [2800°F (1810 K)] during the one hour period 375–435 min. after scram. The maximum debris temperature predicted for the expedestal region during this period is 2706°F (1759 K) for the metal layer at time 418 min.; the calculated debris temperatures decrease rapidly after this peak.

Conclusions regarding the effect of the debris-shell interface upon continued integrity of the drywell shell pressure boundary cannot be reached without additional calculations to determine the thermal response of the shell. Although the predicted debris temperatures are clearly not high enough to cause shell melt-through, failure of the shell pressure boundary through loss of strength is possible. [Because of the uncertainty of this failure mechanism, a flow path between Cells 6 and 10 (lower expedestal region to secondary containment) modeling this failure was not allowed in the current analysis. As described earlier, thermally induced failure of the drywell head seals is modeled and is calculated to occur at time 593 min.] A detailed thermal and stress analysis should be performed for the drywell shell throughout the region of contact with the hot debris to address this issue. It is for this purpose that the time-dependent debris conditions in the expedestal region together with the internal pressure loading of the drywell shell as calculated in this study are provided in Table 4. In particular, this detailed information pertaining to the calculated conditions at the interface during the period of elevated debris temperature is intended for use by interested parties who desire to perform shell response calculations with codes such as HEATING-6 or TAC-2D.

As mentioned previously, the CONTAIN calculations for this case without drywell sprays were terminated at time 900 min. (15 h) after scram. Approximately 98% of the reactor vessel bottom head debris has become molten and left the vessel by this time, and most of the lower portion of the bottom head wall has been subsumed into the debris on the drywell floor. In the

expedestal region, the base of the metal layer is predicted to have sunk 12.9 inches (32.7 cm) beneath the original level of the floor. All of the zirconium metal has long since oxidized, and the metal layer consists only of the frozen (but still very hot) constituents of stainless steel, whose oxidization by gases released by the continued ablation of concrete is slow. Overlying the 9.5-inch (24.2-cm) thickness of frozen metal is a 15.6-inch (39.6 cm) thickness of oxide slurry at a temperature of 2471°F (1628 K), extending to a height of 12.3 in. (31.1 cm) above the original level of the floor. Since the debris pour from the reactor vessel is for all practical purposes terminated at this point, it is reasonable to assume that this is the maximum height that the debris would reach against the drywell shell. Continuation of the CONTAIN calculation to times beyond 900 min. would be expected only to predict that the frozen metal slug and its overlying oxide slurry would continue to slowly sink into the concrete remaining beneath the debris.

4. REMAINING DEFICIENCIES AND UNCERTAINTIES IN CURRENT ANALYSIS

Although the advanced capabilities provided by CONTAIN Version 1.1 greatly improve the efficacy of the code for BWR severe accident applications, the results of this work have made it clear that there are several remaining areas where the present capability must again be expanded if the code is to become adequate for BWR Mark I containment severe accident calculations. Major areas include:

1. Improved representation of concrete degassing. Within the latest released version (1.1) of CONTAIN, none of the gas (H_2O and CO_2) stored in the concrete is released unless and until the temperature of the overlying debris is sufficient to cause ablation. Clearly, this is inadequate during certain times during the accident sequence when the debris cools to below the ablation temperature. It is expected that some degassing of the concrete would occur and would indirectly provide an energy source to the debris via chemical reaction of the gas with unoxidized zirconium.

   The calculations discussed in this paper were performed with an advanced version of CONTAIN provided to the BWRSAT Program at ORNL by the code development staff at SNL. This advanced version partially corrects for the above degassing deficiency. It allows for degassing in the absence of ablation via the use of calculated 1-dimensional concrete temperature profiles and user prescribed temperature release ranges for H_2O (bound and evaporable) and CO_2. While this is a large step forward, it is also desirable that the CONTAIN code be further improved to provide accurate representation of the effects of concrete degassing ahead of the ablation front during periods of unsteady concrete ablation. Although the additional gas release due to accurate modeling of degassing during periods of rapidly increasing debris temperature may be only a fraction of the gas release due to ablation, there are significant periods of time during the present calculation when the metal oxidation reactions in the debris are gas-starved. Therefore, any additional gas release from the

concrete during these periods would be reflected in higher metal oxidation rates and higher temperatures. It is recommended that these advanced degassing models be included in future released versions of CONTAIN.

2. Representation of debris melting. The algorithms for determination of the state of the debris components in the CORCON module of the current released version of CONTAIN are very deficient for BWR severe accident applications. Debris melting is characterized by a determination of solidus and liquidus temperatures applicable only to the vertically separated layer configuration assumed by the CORCON model. Within the metal layer, a tertiary phase diagram is used to determine the melting temperature of the stainless steel according to the relative amounts of its constituent iron, nickel, and chromium. As long as stainless steel is present (there would be an enormous amount of stainless steel in BWR debris), the presence of zirconium metal is ignored and the melting temperature of the metal layer is set equal to the melting temperature of the stainless steel. In actuality, the zirconium metal would be expected to enter into the formation of a eutectic mixture with much of the stainless steel.

   For the oxide layer, the ZrO_2 and UO_2 components are grouped as "fuel" oxides while the oxides created by concrete decomposition are treated separately. A simple phase diagram that provides a melting temperature for a ZrO_2-UO_2 mixture based upon the relative mole fractions is provided within the code for the fuel oxides. The composition and melting temperature of the fuel oxides is combined with that of the concrete oxides to determine the resulting solidus and liquidus temperatures of the oxide layer.

   Difficulty arises with the simple CORCON phase representation for the ZrO_2-UO_2 mixture in that the lowest melting temperature on the diagram is 4625°F (2825 K), which occurs at 56 mole percent ZrO_2. For example, if the BWRSAR code were to predict a pour of molten ZrO_2-UO_2 eutectic at 4352°F (2673 K), the CORCON module within CONTAIN would, upon receipt of this pour, recognize it to be frozen. Thus, the latent heat of fusion for the pour would be lost from the calculation.

   Therefore, in order to perform the calculations reported here, it was necessary to implement a local (ORNL) code modification to reduce the melting temperature of the ZrO_2-UO_2 mixture recognized by CONTAIN/CORCON to 4350°F (2672 K). With this local modification, CONTAIN/CORCON recognizes the molten oxides pouring from the reactor vessel to be molten. It is recommended that modifications be installed in future versions of CONTAIN/CORCON to provide a more realistic representation of the Zr-UO_2 phase diagram or at least, to provide the code user with the ability to set the oxide mixture melting temperature by code input.

3. Representation of B_4C powder. Although there is a significant amount of B_4C powder within the BWR control blades [about 12 lbs (5.4 kg) per blade], the current CONTAIN/CORCON module gives no consideration to the

effect of boron carbide powder upon the core debris or its interaction with the concrete floor. It is recommended that appropriate models, based upon available experimental data, be implemented.

4. Spreading of debris on the drywell floor. There are no models in the current version of CONTAIN to simulate the lateral spreading over the drywell floor of molten bottom head debris released from the reactor vessel. Such a capability should be developed and implemented into CONTAIN. The most important benefit to be gained from a mechanistic debris spreading model is the improved calculation of the oxidation of metals on the drywell floor. As discussed in Section 2 of this paper, metal and oxide debris pours were prescribed for the various regions of the drywell floor based on the spreading analysis developed by Kazimi and the physical state of the debris as it left the failed reactor vessel. For the metals leaving the reactor vessel, this means that independent but simultaneous metal sources appear in the CORCON calculations for inpedestal and expedestal areas. This is nonrealistic because fresh metal would appear first in the inpedestal region beneath the failed reactor vessel and then flow through the pedestal doorway into and around the expedestal region, becoming progressively oxidized along the way. Thus, the chemical energy release in the expedestal region would be greater in the vicinity of the expedestal doorway and less in the more remote areas of the drywell floor. As shown in Section 3, it is this chemical energy release that establishes the maximum temperature of the bulk debris adjacent to the drywell shell.

5. Debris Layer Structure.

   a. The debris layer structure as currently modeled in CORCON is based upon an assumption that individual layers of oxides and metals always exist. During periods of rapid ablation, gas sparging through molten debris makes this debris layering assumption questionable. It is recommended that the CORCON module be modified so that the mixing of the metals and oxides can be calculated automatically or at least controlled with user input. It should be recognized that this in turn will lead to questions concerning the large uncertainties in the chemical and thermophysical environment existing in such a mixture of metals and oxides.

   b. A second change should be implemented in CORCON with respect to the processing of debris added via debris source tables. At present, the new debris is added to the uppermost layer of the previous debris and the temperature of the added debris is immediately equilibrated with the average temperature of the upper layer. For massive upper layers that are calculated to be completely frozen, addition of debris sources in this manner results in temperature gradients in the upper layer crust that are of incorrect sign. This is because the CORCON model prescribes that melting of the uppermost layer be from the interior of that layer. This is inconsistent with the physical situation in which the added debris would reside on top of the upper frozen layer, and thus melting of that layer would not be from the interior

but would occur from the upper surface in contact with the newly added debris.

A potential solution to this problem would be to create a new layer within the existing CORCON layering scheme. This new layer should be thin and located at the top of the debris. Heat and mass transfer should be across the interface of the thin layer with the underlying thick layer.

c. A third change in the CORCON layering scheme should be implemented to address a problem associated with modeling the BWR drywell sumps. The BWR Mark I drywell sumps are small (~6 m^3) and hold roughly 10% of the debris expected to leave a failed BWR reactor vessel. Thus, it is probable that the sumps would be completely filled with metallic debris during the initial metallic pours with some metals remaining to overflow onto the rest of the inpedestal drywell floor. When this occurs, there are two radically different characteristic geometries with which the metal layer is simultaneously associated. The problem in the current application of CORCON is the way in which the crusting model is implemented. The crusting model considers individual debris layers and represents them as cylindrical in shape, using layer thickness and layer volume to calculate an equivalent layer cross sectional area and thus an equivalent layer radius. For the situation described previously with the metals overflowing the sumps, the code simply adopts a cross-sectional area between that of the sumps and that of the inpedestal floor area. As a result of this approach, the crusting model cannot arrive at crusting estimates appropriate for either the sump or the inpedestal geometry. Since debris crusting is a dominant resistance to heat loss from the debris, a deficiency in this model is not of a minor nature. For the calculations performed for this paper, the sump volume was conserved by user input, but the floor area was set to 322 ft^2 (29.9 m^2) – the inpedestal cross-sectional area.

A potential solution to this problem of similar materials in different geometries would be to allow for multiple layers for the same debris. For material filling the sumps and overflowing onto the drywell floor, it seems reasonable to place the material in the sump in one layer and to place the remainder of the debris that overflows onto the floor in another layer. In this way the crusting model as implemented in CORCON would calculate two characteristic crusts for that material – one appropriate for the geometry of the sump and the other appropriate for the inpedestal floor area.

5. SUMMARY

CONTAIN calculations of primary containment response have recently been completed for the Peach Bottom Short Term Station Blackout accident scenario. The specific calculations performed address the debris/concrete interactions that would occur on the floor of the Mark I drywell for the case without drywell sprays. Debris pours from the failed reactor vessel were taken from BWRSAR analyses of the in-vessel response during this scenario.

Three separate CONTAIN calculations were required in order to perform the containment response analysis. The initial CONTAIN calculation addresses the containment response during the time frame 255–375 min. when the debris leaving the reactor vessel via failed bottom head penetrations is expected to remain in the inpedestal region of the drywell floor. The second CONTAIN calculation concerns the time frame of the initial debris spread into the expedestal area, 375–378 min. The extent of initial debris spreading over the expedestal floor was estimated to be 800 ft^2 (74.3 m^2) and was based on a method proposed by Kazimi.

The reason for the short duration of the second CONTAIN calculation is the rapid pour of debris from the failed reactor vessel during this period and the growing superheat of the metallic debris assumed to spread into the expedestal area. The oxidic debris is initially frozen as it leaves the reactor vessel, and for the period of the second CONTAIN calculation, 80% of the oxidic core debris is retained in the inpedestal area with only 20% assumed to flow into the expedestal area. For the metals, it was assumed that one percent was kept inpedestal due to adhesion upon the surfaces of the frozen oxides. An exception was made for the zirconium metal to model its mixing with the oxides; an additional 10% of the zirconium metal was kept inpedestal so that only 89% of this metal was directed into the expedestal region.

The third CONTAIN calculation concerns the time frame 378 to 900 min., for which debris was spread over the remaining 300 ft^2 (27.9 m^2) of the expedestal area. By 515 min., the oxidic debris leaving the reactor vessel was molten along with the metals so that debris partitioning between the inpedestal and expedestal floor areas was based strictly on the floor areas involved. Thus, 77% of all the oxides and metals was placed expedestal (1100 ft^2) while 23% of all the metals and oxides was placed inpedestal (322 ft^2). Prior to time 515 min., debris partitioning was the same as the second CONTAIN calculation.

Results of the CONTAIN analysis indicate that the drywell head flange seals would fail due to thermal degradation at time 593 min. Because the drywell pressure is 126 psia at the time of predicted head seal failure, the head is calculated to lift with the resulting leakage area of 15.5 $in.^2$ (0.010 m^2). The resulting leakage flow would proceed directly into the refueling floor. Smaller leakage flows were calculated after this time due to the pressurization provided by the continuous gas release from the debris/concrete reactions.

Expedestal debris temperatures reach a maximum of 2706°F (1759 K), somewhat below the melting temperature of 2800°F (1810 K) for the carbon steel drywell shell. Although shell burn-through is not indicated, shell integrity is still in question as failure may occur by loss of strength. The debris conditions adjacent to the shell as well as the containment pressure are reported so that more detailed thermal and stress analysis may be performed.

Ablation of the reactor pedestal wall is significant. Results indicate that about 30% of the reactor pedestal thickness is consumed by ablation from

the inpedestal debris. Although not calculated by the expedestal debris/concrete analysis, it is believed that a similar amount of ablation may occur on the outer surface of the pedestal due to attack by expedestal debris.

Cumulative gas release from the debris at the end of the calculation totals 1717 lb-moles. Of this, 1135 lb-moles or 66% of the released gas is H_2 while 485 lb-moles or 28% is CO. Thus, 94% of the released gas from the debris entering the drywell atmosphere is combustible. This has some important ramifications regarding the performance of the secondary containment should the primary containment fail.

Finally, several deficiencies have been identified in the CONTAIN adaptation of CORCON that should be addressed for future best-estimate BWR applications. These include: (1) representation of concrete degassing during periods of unsteady concrete ablation, (2) improved representation of debris melting behavior, (3) chemical and thermophysical representation of boron carbide, and (4) development of an automatic debris spreading model. In addition, three deficiencies have been identified concerning the layer structuring assumed by the CORCON module of CONTAIN. First is the strict adherence to the layering approach during periods of rapid gas sparging through the debris; it is probable that the debris is uniformly mixed. Second is the way in which debris sources are added to the upper layer of the debris. If the upper layer is thick and completely crusted (i.e., frozen), incorrect temperature profiles may be calculated in the frozen layer. A third deficiency concerns the inappropriate method used by CORCON in the determination of radial crusts for layers that experience drastic changes in geometry. The particular BWR application where this problem is most apparent occurs when trying to model the small drywell sumps. In this situation, it may be possible for either metallic debris or oxidic debris to completely fill the sumps and to overflow onto the inpedestal drywell floor. However, the crusting model calculates radial crusts that are not appropriate for either the sumps or for the inpedestal floor. Clearly, the way to resolve this problem is to allow for multiple layers of the same debris.

6. REFERENCES

1. K. K. Murata et al., *Users Manual for CONTAIN 1.1 - A Computer Code for Severe Nuclear Reactor Accident Containment Analysis*, SAND 87-2309 (to be published).

2. S. A. Hodge and L. J. Ott, *BWRSAR Calculations of Reactor Vessel Debris Pours for Peach Bottom Short-Term Station Blackout*, presented at 16th Water Reactor Safety Information Meeting, October 27, 1988.

3. M. S. Kazimi, "On the Liner Failure Potential in Mark-I BWRs," Department of Nuclear Engineering, Massachusetts Institute of Technology, (to be published in *Nuclear Science and Engineering*).

4. CBI NA-CON, Inc., "Mark I Containment Severe Accident Analysis," for the Mark I Owners Group (April 1987).

5. T. L. Bridges, "Containment Penetration Elastomer Seal Leak Rate Tests," NUREG/CR-4944, SAND87-7118, July 1987.

Table 1. Comparison of the constituent weight fractions of Peach Bottom concrete vs high limestone concrete

Constituent	Peach Bottom	High Limestone
Al_2O_3	0.009	0.016
CaO	0.338	0.454
CO_2	0.206	0.357
SiO_2	0.358	0.036
Free H_2O	0.045	0.039
Bound H_2O	0.027	0.020
Other	0.017	0.078
	1.000	1.000

Table 2. Cumulative gas release at termination of calculation for Peach Bottom Station Blackout with ADS actuation and limestone common sand concrete Time 900 min.

	lbs	lb-moles
Gas release from concrete		
CO_2	61,555	1399
H_2O	21,339	1184
	82,894	2583
Gas release from debris surface		
CO_2	2,180	49.5
H_2O	847	47.0
CO	13,592	485.3
H_2	2,289	1135.6
	18,908	1717.4

Table 3. Debris configurations before and after spreading at time 375.0 min for Peach Bottom Short-Term Station Blackout with ADS actuation and limestone common sand concrete

Before Spreading
Inpedestal only (322 ft²)

(Inches)

3.13 _____ Tsolidus

oxides 2522°F
metals 2690°F

Floor 0.00 -----Oxides----- Toxide = 2654°F
Tmetal = 2536°F

Mass oxides = 73,971 lbm
Mass metals = 101,610 lbm

-7.01 _____

Metals

-16.26 _____

After Spreading:

Inpedestal (322 ft²)		**Expedestal (800 ft²)**	
0.98	_____	_____	.94
		Oxides	
		_____	.45
Floor 0.00	-----Oxides-----	-----Metals-----	0.00 Floor
		_____	-.01
-7.98	_____		
	Metals		
-16.27	_____		
Toxide = 2586°F		Toxide = 2592°F	
Tmetal = 2586°F		Tmetal = 2590°F	
Mass oxides = 65,847 lbm		Mass oxides = 8,442 lbm	
Mass metals = 90,199 lbm		Mass metals = 11,612 lbm	

Table 4. Expedestal debris conditions for Peach Bottom Short Term Station Blackout with ADS actuation and limestone common sand concrete

Time (min)	Zbot (in.)	$Z_{MET/LOX}$ (in.)	$Z_{LOX/ATM}$ (in.)	Mass metals (lbs)	T_{METALS} (°F)	$T_{SOLIDUS}$ METALS (°F)	LOX-mass light oxides (lbs)	T_{LOX} (°F)	$T_{SOLIDUS}$ (LOX) (°F)	Drywell Pressure (psia)
375.0	0.00	0.45	0.94	11,610	2590	2690	8,442	2592	2523	62.0
375.5	-0.04	0.46	1.00	12,860	2622	2690	9,298	2628	2526	63.7
376.0	-0.09	0.47	1.06	14,290	2654	2691	10,340	2659	2529	64.3
376.5	-0.14	0.48	1.14	15,810	2681	2691	11,430	2687	2531	64.6
377.0	-0.20	0.48	1.21	17,300	2693	2691	12,610	2692	2831	64.8
377.5	-0.26	0.48	1.28	18,810	2694	2692	13,830	2693	2531	65.0
378.0	-0.32	0.48	1.35	20,310	2695	2692	15,060	2695	2531	65.2
379.0	-0.42	0.40	1.20	25,450	2677	2692	19,610	2679	2538	65.7
380.0	-0.52	0.39	1.31	28,600	2685	2692	22,160	2685	2536	66.1
381.0	-0.63	0.39	1.42	31,890	2691	2692	24,770	2692	2534	66.5
382.0	-0.75	0.39	1.54	35,340	2693	2693	27,520	2692	2531	66.9
383.0	-0.87	0.39	1.66	38,970	2694	2693	30,310	2693	2528	67.2
384.0	-0.99	0.39	1.78	42,740	2696	2694	33,100	2695	2526	67.6
385.0	-1.11	0.38	1.90	46,460	2697	2694	35,880	2695	2523	68.0
386.0	-1.23	0.38	2.02	50,140	2697	2695	38,660	2696	2521	68.3
387.0	-1.35	0.38	2.14	54,010	2698	2695	41,440	2697	2519	68.7
388.0	-1.47	0.38	2.26	57,830	2699	2695	44,210	2697	2518	69.1
393.0	-2.07	0.40	2.89	77,700	2701	2696	58,030	2699	2510	70.5
398.0	-2.68	0.59	3.69	100,360	2701	2696	71,700	2698	2505	72.2
403.0	-3.28	0.70	4.42	127,000	2702	2696	85,720	2699	2504	74.3
408.0	-3.89	0.43	4.75	136,100	2703	2699	99,190	2700	2499	76.5
413.0	-4.50	-0.03	4.89	138,300	2704	2702	112,200	2702	2493	78.8
418.0	-5.10	-0.51	4.98	139,500	2706	2706	125,200	2695	2489	80.9
423.0	-5.54	-0.86	4.99	142,300	2680	2709	134,500	2651	2486	83.2
428.0	-5.87	-0.71	5.08	146,500	2647	2713	141,100	2609	2483	85.0
433.0	-6.16	-0.86	5.20	151,300	2630	2716	147,000	2575	2482	86.8
438.0	-6.41	-0.95	5.33	157,300	2538	2719	151,300	2545	2475	88.8
443.0	-6.59	-0.96	5.42	169,900	2472	2723	154,500	2509	2467	90.5

$T_{SOLIDUS}$ = Mixture temperature at which melting begins

LOX = Light oxides

HOX = Heavy oxides

Z = Elevation relative to original floor surface

MET/LOX = metal - light oxide interface

LOX/ATM = light oxide - atmosphere interface

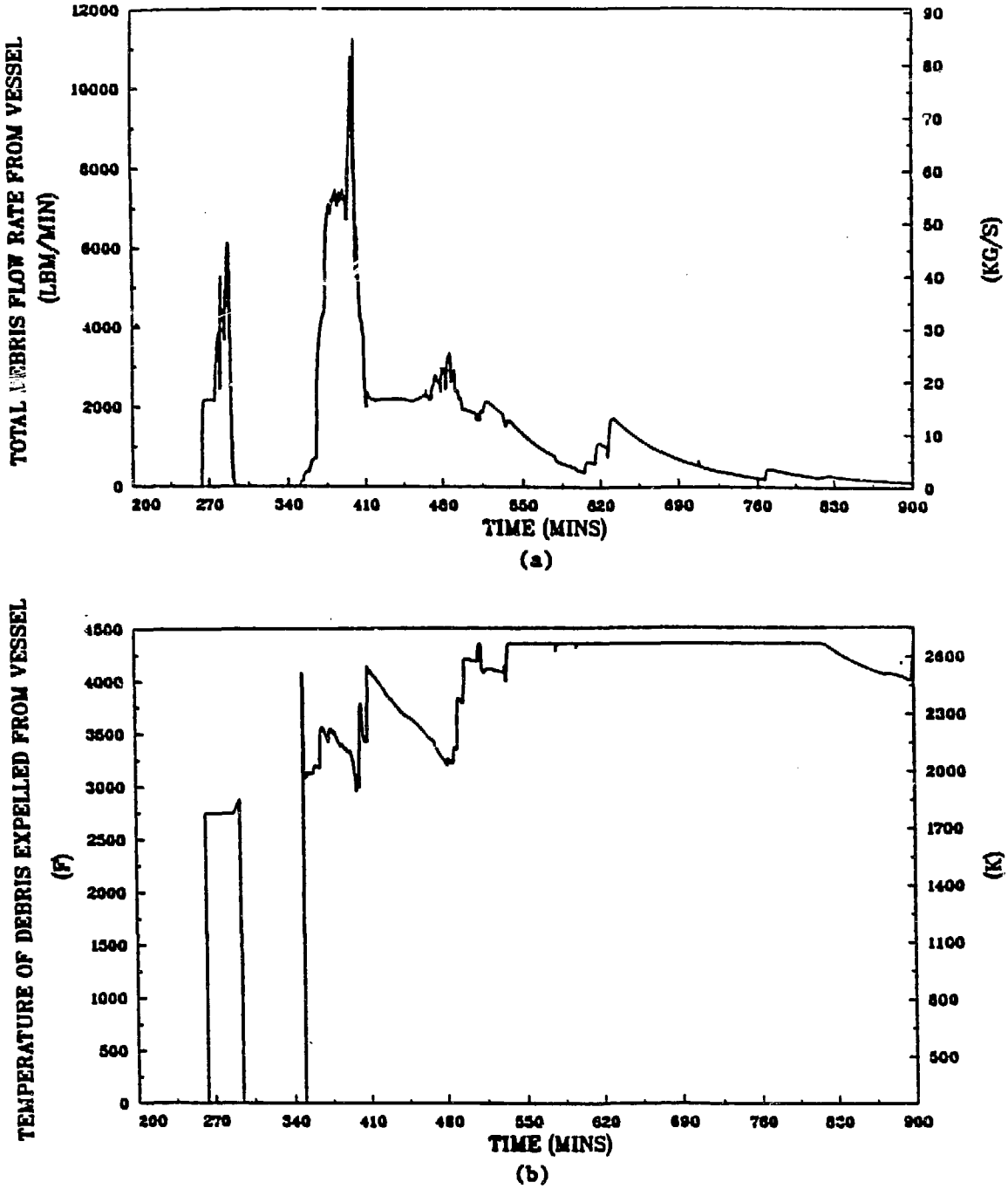

Fig. 1. Flow rates and temperatures of debris pours from the reactor vessel bottom head as predicted by the BWRSAR code for the short-term station blackout accident sequence with ADS at a unit of the Peach Bottom Atomic Power Station.

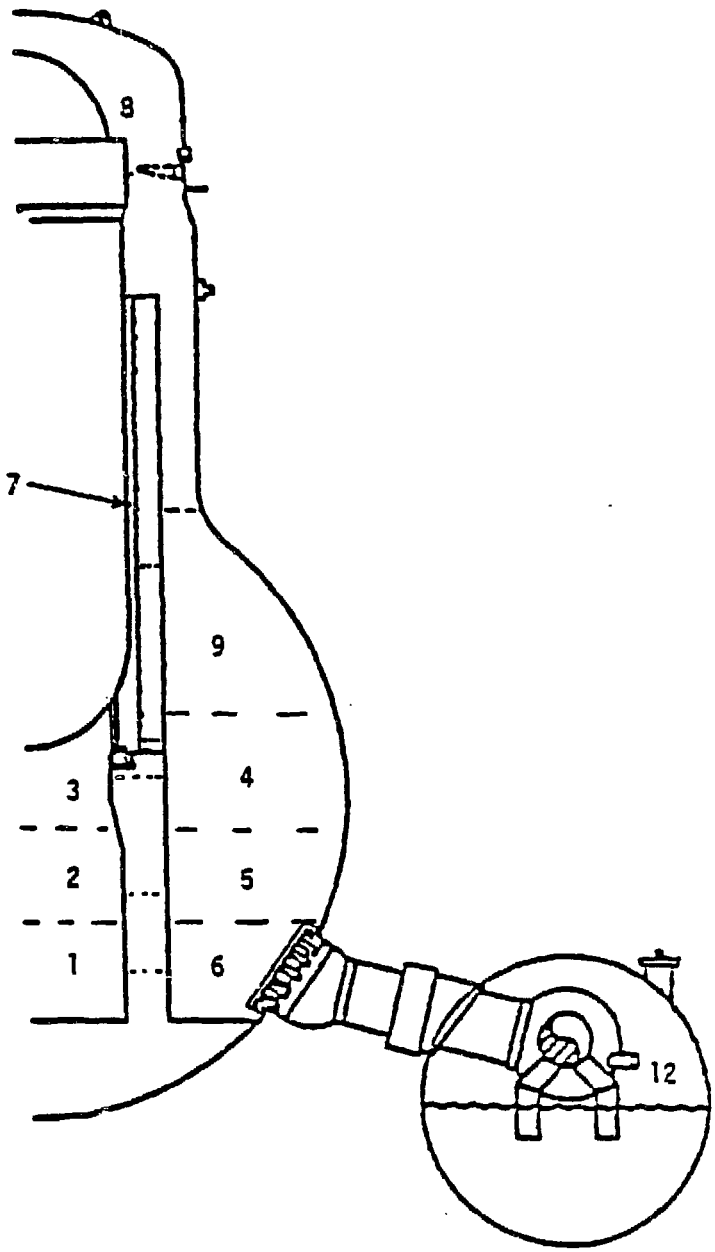

Fig. 2. BWRSAT Program Nodalization for the BWR Mark I Primary Containment. Not shown are cells 10 (secondary containment) and 11 (outside environment), which make up the balance of the complete CONTAIN model used for the Peach Bottom Calculations.

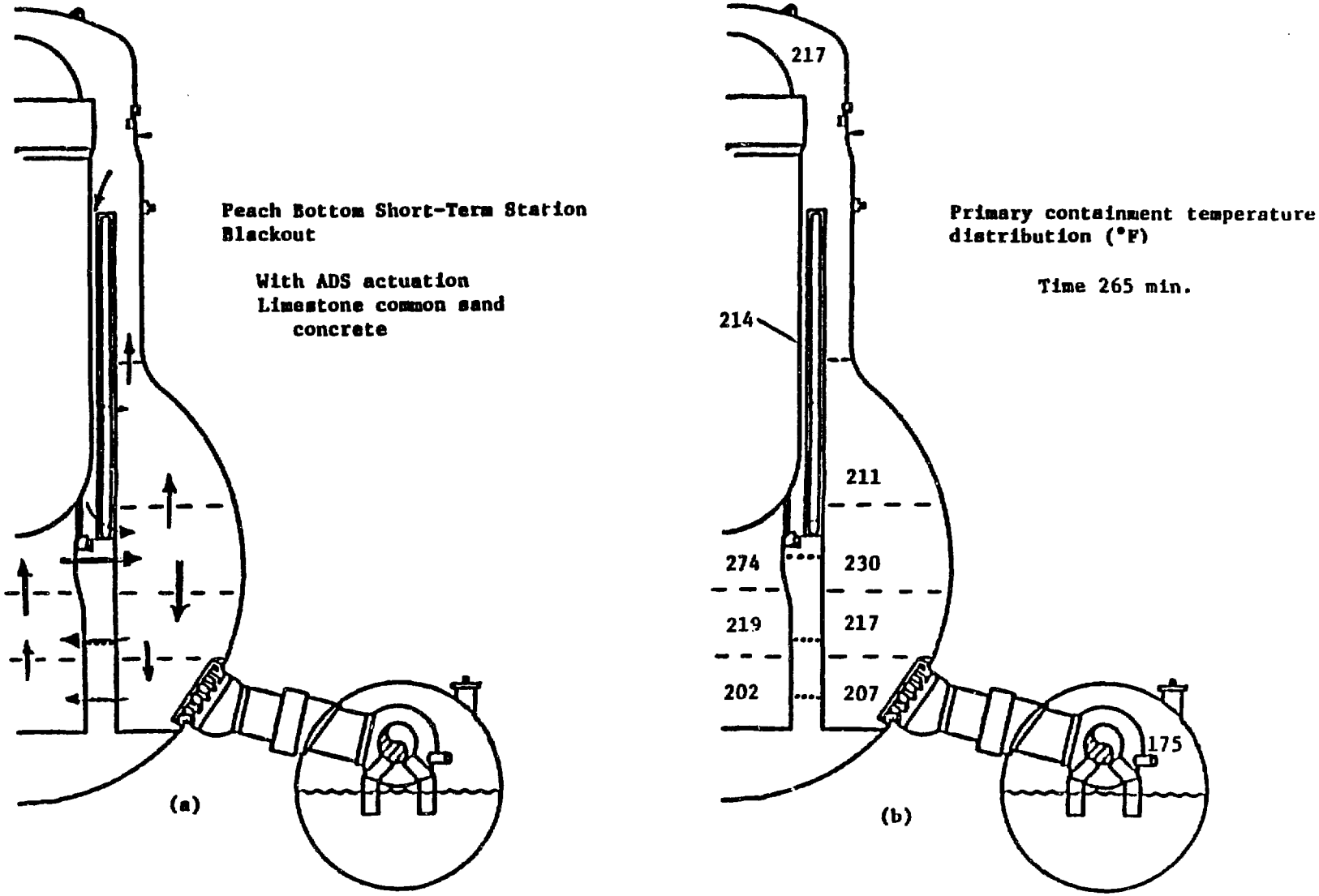

Fig. 3. Drywell intercell flows and cell temperatures as predicted by CONTAIN at 10 minutes after reactor vessel bottom head penetration failure and just before the inpedestal CORCON calculation is initiated.

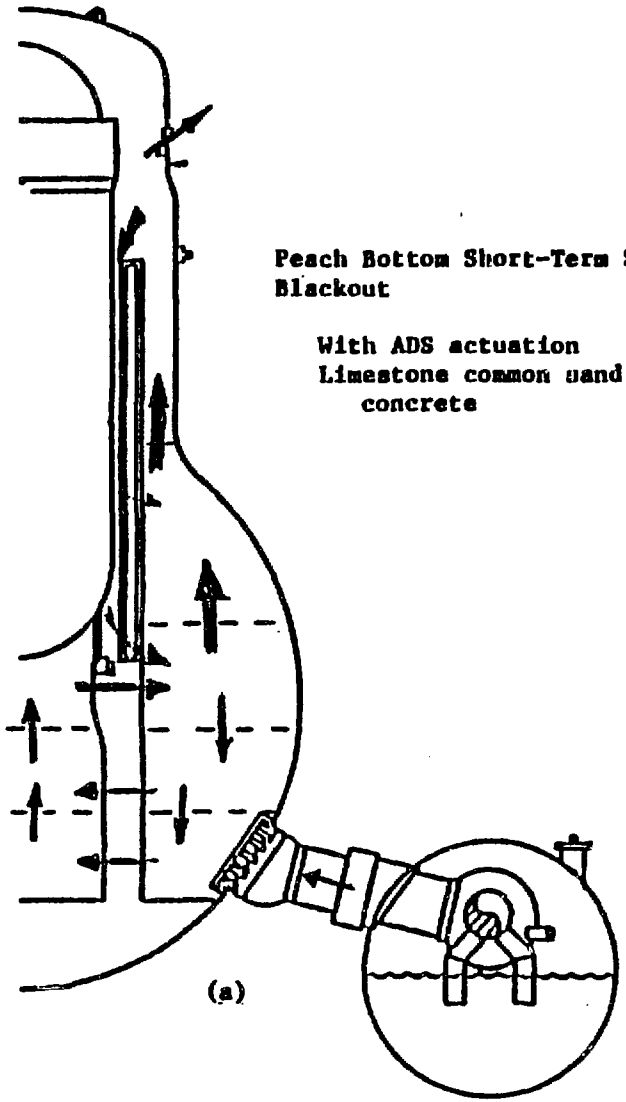

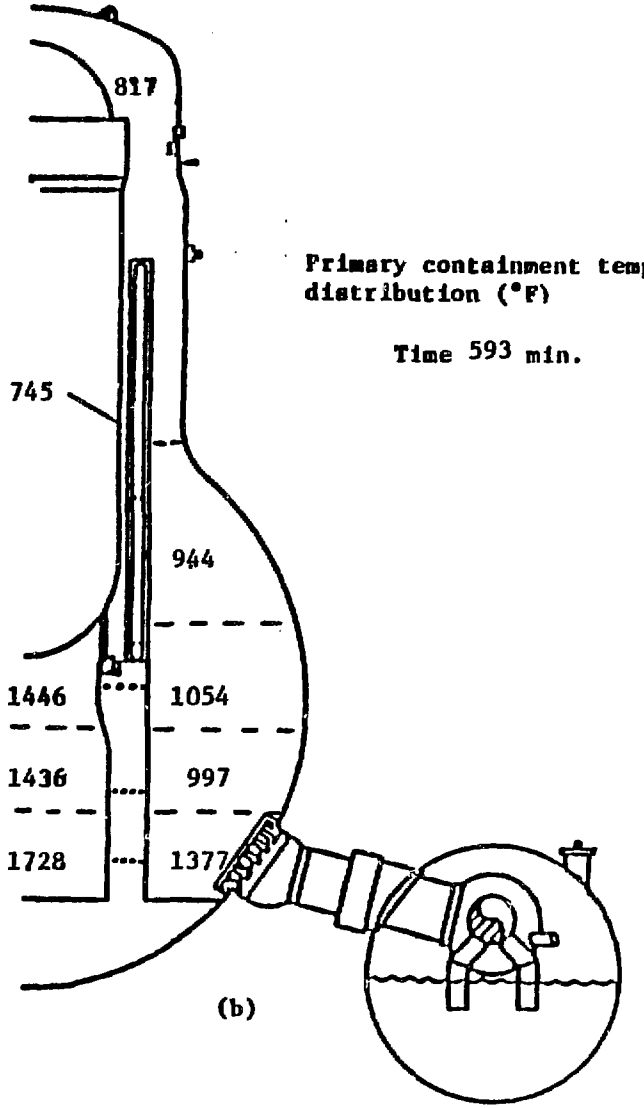

Fig. 4. Drywell intercell flows and cell temperatures as predicted by CONTAIN 0.8 minutes after drywell head flange leakage begins. The leakage is induced by a combination of high drywell pressure, which lifts the head and high temperature, which degrades the seals.

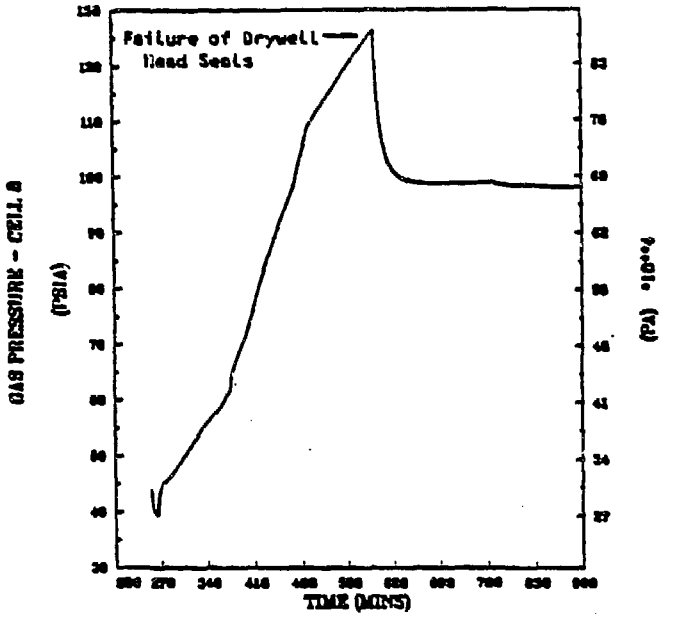

(5)

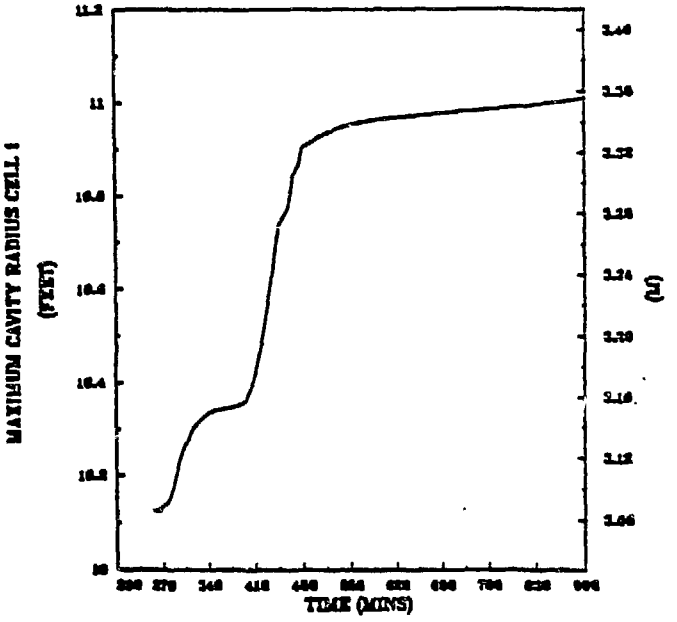

(6)

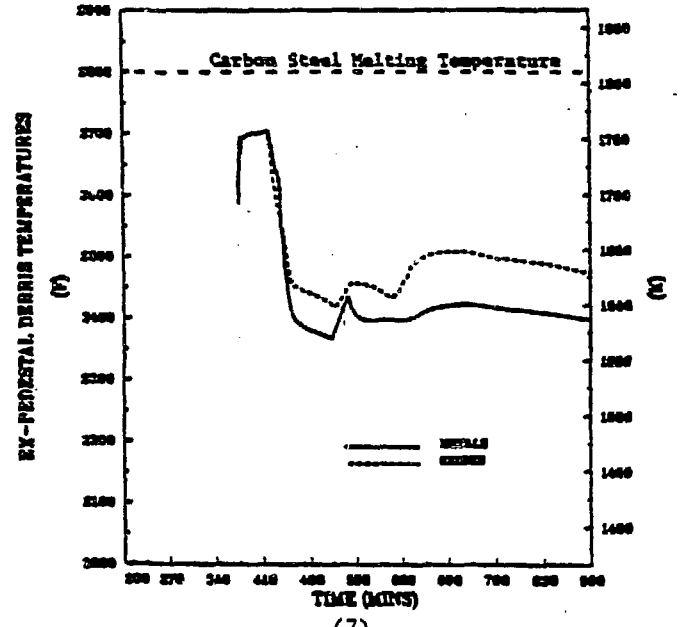

(7)

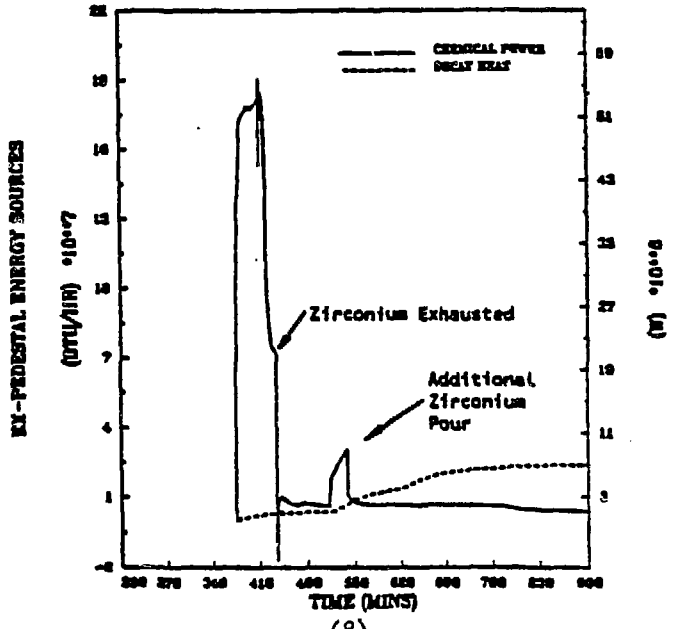

(8)

Figs. 5–8. Selected parameters relative to maintenance of drywell shell pressure boundary integrity for Peach Bottom Short-Term Station Blackout with ADS actuation. The first spread of debris into the expedestal region occurs at time 375 minutes. The floor is modeled as limestone common sand concrete without overlying water.

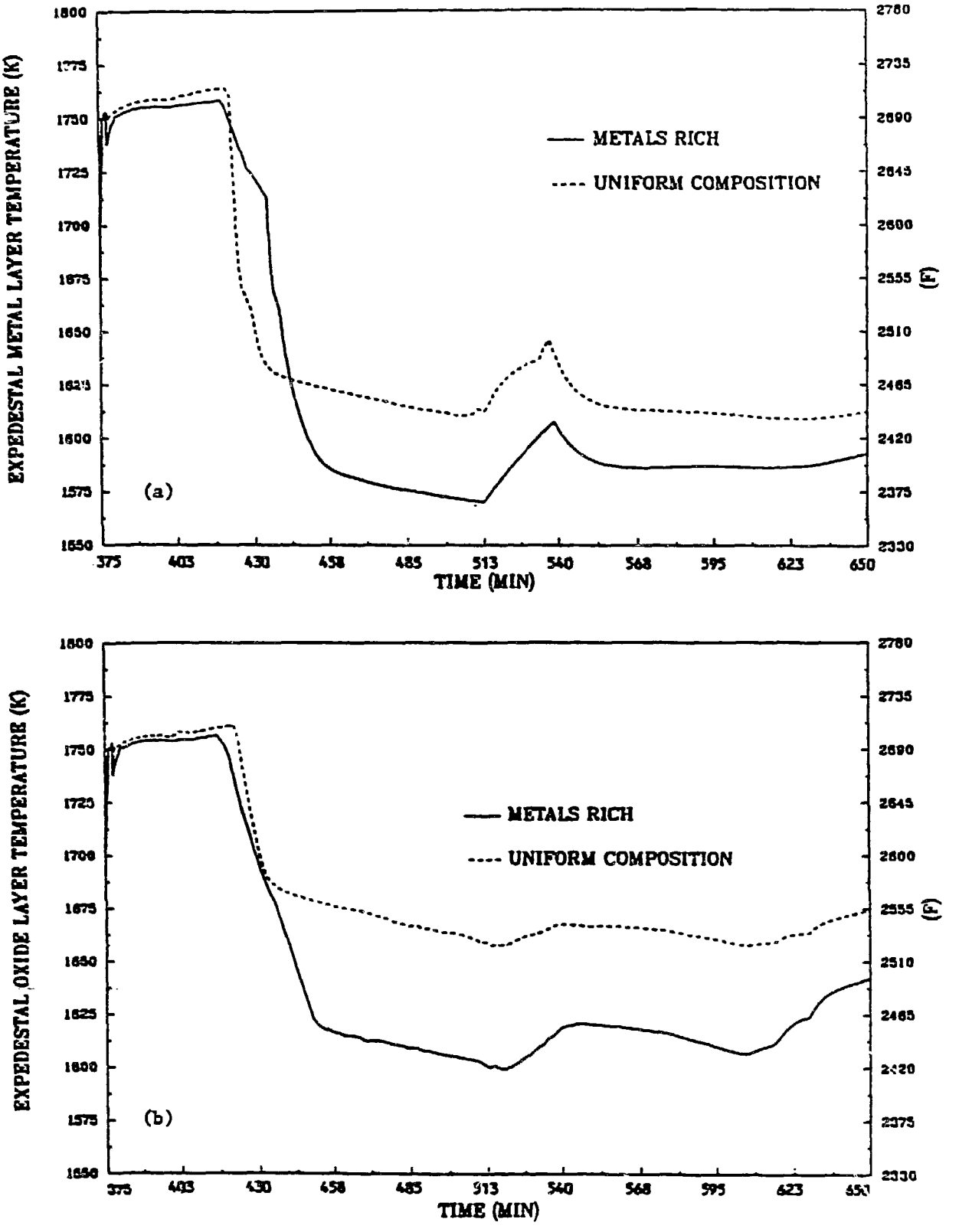

Fig. 9. Comparison of the debris layer temperatures in the expedestal region for the case of best-estimate (metals rich) spreading vs. the case with equal spreading of oxides and metals.